Published in final edited form as:
J Memb Sci. 2014 May 1; 457: 39–49. doi:10.1016/j.memsci.2014.01.033.

Development of Bench and Full-Scale Temperature and pH Responsive Functionalized PVDF Membranes with Tunable Properties

Li Xiao[1], **Austin Isner**[1], **Krysta Waldrop**[1], **Anthony Saad**[1], **Doreen Takigawa**[2], and **Dibakar Bhattacharyya**[1,*]

[1]Department of Chemical and Materials Engineering, University of Kentucky, Lexington, KY 40506, USA

[2]Sepro Membranes, Inc. Oceanside, CA 92056, USA

Abstract

Temperature and pH responsive polymers (poly(N-isopropylacrylamide) (PNIPAAm), and polyacrylic acid, PAA) were synthesized in one common macrofiltration PVDF membrane platform by pore-filling method. The microstructure and morphology of the PNIPAAm-PVDF, and PNIPAAm-FPAA-PVDF membranes were studied by attenuated total reflectance Fourier transform infrared (ATR-FTIR), thermogravimetric analysis (TGA), scanning electron microscopy (SEM) and atomic force microscopy (AFM). The membrane pore size was controlled by the swelling and shrinking of the PNIPAAm at the temperature around lower critical solution temperature (LCST). The composite membrane demonstrated a rapid and reversible swelling and deswelling change within a small temperature range. The controllable flux makes it possible to utilize this temperature responsive membrane as a valve to regulate filtration properties by temperature change. Dextran solution (M_w=2,000,000g/mol, 26 nm diameter) was used to evaluate the separation performance of the temperature responsive membranes. The ranges of dextran rejection are from 4% to 95% depending on the temperature, monomer amount and pressure. The full-scale membrane was also developed to confirm the feasibility of our bench-scale experimental results. The full-scale membrane also exhibited both temperature and pH responsivity. This system was also used for controlled nanoparticles synthesis and for dechlorination reaction.

Keywords

polymerization; Poly(N-isopropylacrylamide); polyacrylic acid; tunable separation; nanoparticle synthesis

*Corresponding Author: Dr. D. Bhattacharyya University Alumni Chair Professor Department of Chemical & Materials Engineering University of Kentucky Lexington, KY 40506 db@engr.uky.edu Phone No.: 859-257-2794 Fax: 859-323-1929.

1. Introduction

Environmentally sensitive polymers have gained considerable attention in areas ranging from new material designs to drug delivery and composite biomaterials[1-4]. These polymers can transform between swollen and shrunk state reversibly in response to environmental conditions such as pH, temperature, light, the nature of solvent and added chemicals[5-7]. For example, poly(acrylic acid) (PAA) is a typical polyelectrolyte and particularly used in sensing and modulating external chemical signals due to the conformation change based on pH change and ionic strength of the aqueous media[8]. Poly(N-isopropylacrylamide)(PNIPAAm), on the other hand, is the most widely studied temperature responsive polymer. It exhibits remarkable and reversible hydration-dehydration changes in temperature near lower critical solution temperature (LCST) at around 32°C[9]. Below the LCST, the polymer network is hydrophilic due to the formation of the hydrogen bonding between amide groups on the PNIPAAm chain and water molecules. When the temperature increases higher than the LCST, the hydrogen bonds are broken and water is expelled from the network leading to the hydrophobic network[10, 11]. These smart polymers are considered to have great potential in a wide variety of applications, such as, controlled drug delivery, chemical separation, water treatment, sensor and bioreactors[12-14].

However, these polymers, unfortunately, usually lack mechanical strength to be used alone for a particular application. Therefore, responsive membranes with the combination of a responsive hydrogel and a porous substrate membrane have been developed [15, 16]. The porous supports can provide mechanical strength and dimensional stability. Several micro-porous supports have been reported including poly(vinylidene fluoride) (PVDF)[13], polyethylene (PE)[17], polypropylene (PP)[18], poly(ethylene terephthalate) (PET)[19], polycarbonate (PC)[20]. PVDF is known to have advantages of good thermal and chemical resistance properties and also the asymmetric structure is known to have lower mass transfer resistances[21]. Our group has already published the formation of PAA hydrogels inside the pores of PVDF membranes for in-situ nanoparticle fabrication and toxic organic remediation[22, 23].

Since temperature responsive polymer is the most easily designed and controlled among these stimuli, thermo-responsive membranes have gained special interest. Most thermo-responsive membranes have been prepared by forming PNIPAAm chains directly in/on porous membranes. The methods reported include UV photo-grafting, plasma modification, irradiation and ion–tracking[24-26]. These macroporous membranes with PNIPAAm hydrogel can act as a valve with controlled or adjusted permeability due to the open and close of membrane pores caused by the shrinking and swelling of PNIPAAm chain according to the temperature changes. In comparison with conventional separation process, this proposed membrane system may have the potential to separate mixtures of molecules with similar molecular sizes through selective adsorption of different molecules based on the modification of hydrophobicity and hydrophilicity by immobilized thermo-sensitive gel[25]. Moreover, the process has both feed and permeate streams, which can allow the continuous flow and allow to collect the permeate with a temperature swing operation. Besides the use of advanced separation, this system also has the potential to water treatment technology[27].

This platform can be used as a support to immobilize metal nanoparticles for catalytic dechlorination of toxic chlorinated organic compounds with the prevention of aggregation, oxidation and potentially tunable reactivity via the change of temperature. On the other hand, the immobilized functional polymers in the membrane support are important for the gating of stimuli-responsive permeability of membranes. Therefore, several important parameters, such as the grafting yield, the morphologies of filled polymer gel, the molecular size of permeate and initial membrane pore size have been reported to play an important role[28] and need to be investigated. For responsive membranes, stable responsive characteristics are also very important and essential.

The synthesis of temperature responsive membranes have been published for the application of controllable drug release. However, the synthesis of both temperature and pH responsive membranes for both separation and reactions based on full-scale membranes hasn't been reported yet. Therefore, the main objectives of this study are: (1) preparation and characterization of PNIPAAm functionalized PVDF membrane; (2) investigation about the temperature responsive on solvent permeation properties; (3) studies of the effects of monomer concentration and cross-linker amount on the temperature responsive permeation flux behavior; (4) the development of both temperature and pH responsive membrane based on full-scale membrane to evaluate the feasibility of continuous manufacture of functionalized membranes and (5) the synthesis of PNIPAAm-PAA-PVDF with immobilized metal nanoparticles for catalytic dechlorination.

2. Experimental

2.1. Materials

All chemicals were used as reagent grade. Hydrophilized polyvinylidene fluoride (PVDF) microfiltration membranes were obtained from Millipore (average pore size: 0.65 m, thickness:125 m, porosity: 70%, diameter: 142 mm) and full-scale PAA-PVDFHE membrane[29] (hydrophilized, average pore size: 0.42 m, PVDF layer thickness: 70 m porosity: 45 55%) was obtained from Sepro Membranes Inc., Oceanside, CA. N-isopropylacrylamide (NIPAAm), N,N'-methylenebisacrylamide (BIS), ammonium persulfate (APS), N,N,N',N'-tetramethylethylenediamine (TEMED), acrylic acid (AA) and ethanol (>99.5%), dextran (M_w=2,000,000 g/mol) were purchased from Sigma-Aldrich. Deionized ultra-filtered water (DIUF) was from Fischer Scientific. Ultra-high purity (UHP) nitrogen gas used in flux experiments was purchased from Scott Specialty Gases.

2.2. Synthesis of PNIPAM-functionalized PVDF Millipore membrane

Although many membranes can be used for this application, PVDF membrane was chosen in this paper because of its chemical resistance properties and good thermal stability[21]. The thermo-sensitive PNIPAAm-PVDF membrane was prepared via pore-filling method by the redox polymerization as reported in the literatures [30, 31]. The polymerization was conducted in aqueous phase. The polymerization solution contained 5 wt% NIPAAm (monomer), BIS (cross-linker, added in a 0.1-5% molar ratio of BIS to NIPAAm), and 1% APS (initiator). The solution was purged with nitrogen for 1h. After adding 1% of redox accelerator, TEMED, the PVDF membrane was put into the solution and the reaction

continued for 6h at 25°C. The resulting composite membrane was taken out from the gel carefully and immersed in DIUF overnight. The effects of cross-linker density and monomer concentration were also studied.

The full-scale FPAA-PVDFHE flat sheets (40 inches wide and 300 feet long, 70 m PVDF thickness) were recently developed by joint work with Sepro Membranes Inc., Oceanside, CA. These hydrophilized PVDF membrane support was made with backing fabric to increase material stability. They have fairly uniform geometry, open structure and polymer distribution. The full-scale membrane was post-functionalized with PNIPAAm to get both temperature and pH responsive behavior. It should be noted that unlike the Millipore PVDF membrane, the functionalization of full-scale membrane was by dip-coating method. Therefore, a higher NIPAAm concentration (13wt%) is used to make sure enough polymer formed in the pores. 1 mol% of BIS and 1 mol% of APS with respect to NIPAAm were added to the solution, and the membrane was immersed in the monomer solution for 5 min. The membrane was sandwiched into two glass plates after getting rid of excess solution on the membrane surface and put it in the oven for 2.5h at 70°C. The membrane was washed with DIUF and ethanol for several times, and immersed in DIUF overnight. The schematic for the PNIPAAm functionalization with full-scale FPAA-PVDFHE Sepro membrane (PNIPAAm-FPAA-PVDFHE) is shown in Figure 1. The membrane description and their abbreviation are shown in Table 1.

2.3. Attenuated total reflectance Fourier transform infrared (ATR-FTIR)

Attenuated total reflectance Fourier transform infrared (ATR-FTIR) (Varian 7000e) was used to determine the presence of functional groups in PNIPAAm-PVDF membrane. The samples were placed on the diamond crystal and the spectrum was obtained between 500 and 4000 cm^{-1} for 32 scans at a resolution of 8 cm^{-1}.

2.4. Scanning Electron Microscopy (SEM)

The surface and cross-section morphology of the blank PVDF and PNIPAAm-PVDF membranes were studied by Hitachi S-4300 Scanning Electron Microscope (SEM). The samples were mounted on the sample studs and a thin layer of gold was sputtered on the sample surface for imaging purpose. The SEM measurements were performed at an accelerating voltage of 10 kV.

The effect of temperature on the morphology of membranes was also investigated. The membranes were swelled in water at temperature 25°C and 40°C for 48h to reach equilibrium, respectively. Then, the membrane was taken out and immediately put it in liquid nitrogen, and dried under freeze drying. The dry samples were used for SEM analysis.

2.5. Thermal analysis

The thermal properties of the PNIPAAm-PVDF membrane were measured by thermogravimetric (TG) analysis and differential scanning calorimetry (DSC). For TG analysis, the samples were heated up to 600°C with a rate of 10°C/min under dry nitrogen atmosphere by using a TGA 2050 thermo-gravimetric analyzer (TA Instrument, USA). For DSC analysis[13, 30], the samples were immersed in distilled water at room temperature for

at least two days to reach a swollen state. About 10 mg swollen sample was placed inside a hermetic aluminum lid. The thermal analyses were performed from 25 to 50 °C on the swollen samples by using DSC An empty pan was used as reference. Q200 (TA instrument USA) under dry nitrogen atmosphere with a flow rate of 50 mL/min and a heating rate of 0.5°C/min and 2.5°C/min to check the effect of heating rate.

2.6. Atomic force microscopy (AFM)

The membrane surface was also characterized by AFM (Agilent PicoPlus 3000) using a resonance frequency of approximately 150 kHz in tapping mode. The average roughness (the average deviation of the peaks and valleys height from the mean value) was determined on 5 m × 5 m membrane area. All AFM images were processed and presented using Gwyddion software.

2.7. Temperature-responsive flux measurements

The water permeability was measured at different temperatures to study the temperature responsive flux behavior of PNIPAAm-PVDF Millipore membranes and PNIPAAm-FPAA-PVDFHE Sepro membrane. The tested membrane was mounted in a stirred cell (Millipore). The stirred cell containing the feed water was kept in constant temperature for at least 1.5 h by electrical heating tape with a digital thermocouple to continuously monitor the internal feed temperature at the membrane-solution interface. The cell was pressurized using pure nitrogen. Once the membrane flux reached steady-state, volume flux was measured in triplicates by recording the volume passed in a given time interval. A final run was conducted by adjusting the feed temperature back to 30°C to test for reversibility.

2.8. Dextran rejection

The solution consisting of 2 g/L dextran (M_W = 2,000,000 g/mol) was fed into a convective flow cell and was equilibrated at 30°C for 1h at 1.4 bar. After first run, the DIUF feed was replaced with dextran solution at 30.0°C to wash the membrane. Then, a second rejection study was conducted at 34.0°C. All experiments were conducted in triplicate and average values are given. After equilibration, multiple permeate and feed samples were collected for total organic carbon (TOC) and gel permeation chromatography (GPC) analysis.

2.9. Total organic carbon (TOC) analysis

The total organic carbon was analyzed using a TOC analyzer. Carbon standards were prepared in the range from 1-100 mg/L to generate a calibration curve. Samples were automatically introduced to the TOC analyzer (experimental error <2%). Ultra-high purity nitrogen was used as the carrier gas at 87.0 psi and a flow rate of 150 mL/min.

2.10. Gel Permeation Chromatography (GPC)

Feed and permeate samples (1mL) were analyzed by a Shimadzu HPLC system with a Shimadzu refractive index detector (RID-10A). The gel permeation column used was a Shimadzu (Tokyo, Japan) TSK-GEL G6000PWXl. Column temperature was maintained at 30±1°C. For analysis, the column was operated under isocratic flow conditions of 0.5 mL/min with phosphate buffered saline (PBS) (0.0119M phosphates, 0.137 M NaCl, 0.0027

KCl) (pH 7) as the mobile phase. Before injection, the samples were filtered with 0.45 m PVDF porous membrane.

2.11. Salt rejection through PNIPAAm-FPAA-PVDFHE Sepro membrane

Na_2SO_4 rejection experiments were performed using a stirred membrane cell provided by Millipore with a membrane cross-sectional area of 13.2 cm^2 including a stirring device to minimize the effects of concentration polarization. The effects of Na_2SO_4 concentration on the rejection was also investigated by using 100 mg/L and 1000 mg/L concentration. The sodium concentration was measured with a Varian AA220 series atomic absorption spectrophotometer.

2.12. Metallic nanoparticles synthesis within PNIPAAm-FPAA-PVDFHE membrane

The method for the synthesis of nanoparticles is developed by our group and described anywhere else[22, 23]. Before ion exchange with Fe^{2+}, the membrane was immersed in NaCl/NaOH solution (pH=11.9) overnight to convert –COOH to –COONa. In the next step, the membrane was washed with DIUF until the pH of the effluent became neutral. Then, the membrane was immersed in 200 mL 200 mg/L $FeCl_2$ solution at a pH of 5.5 for 4 h. Nitrogen gas was bubbled to minimize the oxidation of Fe^{2+}. The reduction with sodium borohydride ensured the Fe^0 nanoparticle formation. The membrane was stored in ethanol to prevent the oxidation. For the deposition of second metal (Pd) on the surface of Fe nanoparticles, the membrane was immersed in K_2PdCl_4 solution of ethanol and water (90:10 vol%). The concentration of K_2PdCl_4 solution varied based on the Pd amount desired to be deposited on the Fe nanoparticles. The amount of Fe and Pd immobilized in the membranes during the ion exchange and post coating was quantified using Varian AA220 series atomic absorption spectrophotometer with the wavelength of 386.0nm and 247.6 nm respectively.

3. Results and Discussion

3.1. Functionalized Membrane Characterization

3.1.1 ATR-FTIR spectroscopy of the PNIPAAm functionalized PVDF membrane—The functionalization of the PVDF membranes with PNIPAAm was characterized by ATR-FTIR spectroscopy as shown in Figure 2. The characteristic absorption band for CF_2 of blank PVDF appears at 1120-1280 cm^{-1} [32]. Compared with the spectrum of blank PVDF membrane, two new peaks appeared at about 1650 and 1540 cm ^{1} in both spectra of PNIPAAm-PVDF and PNIPAAm-FPAA-PVDFHE composite membrane. The absorption band at about 1650 cm ^{1} belongs to the second amide C=O stretching (amide I) and the band at 1540 cm ^{1} is corresponding to the N–H stretching (amide II) of the O=C–NH groups in the PNIPAAm chains [24, 26, 33]. The peaks in 1366-1466 cm^{-1} range are corresponding to the symmetrical and asymmetrical bonds of isopropyl groups from NIPAAm. This comparison results verified the formation of PNIPAAm with PVDF membrane support by pore-filling method.

3.1.2 Thermal analysis—The thermal stability of blank PVDF and PNIPAAm-PVDF Millipore membranes were evaluated by TGA, and the resulting TGA curves are presented in Figure S1. The blank PVDF begins to decompose at about 460°C[32], while the

PNIPAAm-PVDF shows a distinct two-step degradation process. This phenomenon is attributed to the degradation of PNIPAAm chains and PVDF main chains at different temperatures. The first major loss of PVDF-PNIPAAm begins at about 400°C, corresponding to the decomposition of PNIPAAm chains[26, 30]. The onset of second major loss occurs at about 460°C, which is attributed to the decomposition of PVDF main chains. Figure S2 shows the thermograms of the PNIPAAm-PVDF membrane. Since the hydrogen bonding between the water solvent and PNIPAAm chains will be broken during the dehydration process upon heating[30], only one endothermic peak is observed as shown in Figure S2. The transition temperature (LCST) determined from the intersection of the baseline and the leading edge of the endotherm and is about 32±0.5°C, which is consistent with the reported LCST of PNIPAAm[11, 13]. Additional information about the effect of heating rate on the LCST measurement can be found in supporting information.

3.1.3 Microstructure and morphology analysis

3.1.3.1 SEM: The morphologies of the blank PVDF and PNIPAAm-PVDF Millipore membranes were examined by SEM shown in Figure 3. The blank PVDF Millipore membrane shows (Figure 3A) a highly porous structure with mostly circular shape and non-uniform pore size. As expected, the functionalized PNIPAAm-PVDF membrane (Figure 3B and C) showed less porosity with small size of pores. The grafted hydrogels were not removed in the rinse treatment, which indicate the strong attachment between the PNIPAAm hydrogel and the PVDF membrane[20]. The microstructure showed strong evidence of the polymerization of NIPAAm onto the membrane.

On the other hand, the surface images (Figure S3A and B) of PNIPAAm-FPAA-PVDF Sepro membranes clearly show that the PNIPAAm was coated on the surface with decrease of pore size. Furthermore, it can be obviously seen from the cross-section images (Figure S3C and D) that the PNIPAAm hydrogel filled in the pores through the whole FPAA-PVDF layer resulting in a denser membrane and less porosity. It should be noted that all the SEM images are obtained under dry conditions. Therefore, the real morphology of PNIPAAm-FPAA-PVDF membranes may be more different from FPAA-PVDF membrane. These results are consistent with the reported methods by using different membrane supports and synthesis techniques [34, 35].

The temperature effect on the structure of composite membrane was also studied and showed in Figure 3B and C. It indicates that the membrane pore size is increased when temperature increases from 25°C (below LCST) to 40°C(above LCST). This phenomenon is consistent with the change in conformation and orientation of the PNIPAAm chain near the LCST. When the temperature is below the LCST, the PNIPAAm hydrogel on the membrane or the inner pores swells and occupies the pore volume, which decrease the effective pore size. Whereas when the temperature above the LCST, the PNIPAAm hydrogel changes to a shrinking state, leading to the increase of the effective pore size. Therefore, by adjusting the initial monomer concentration, the pore-filling density in the membrane support can be controlled, which in turn regulate the temperature responsive behavior as detailed discussed in the following section.

3.1.3.2 AFM: AFM was chosen to characterize the surface morphology of full-scale PVDFHE and functionalized PNIPAAm-FPAA-PVDF Sepro membranes as shown in Figure 4. Average roughness is defined as average deviation of the peaks and valleys from the mean plane and root mean squared (RMS) roughness is the RMS deviation of the peaks and valleys. The untreated PVDF membrane showed a flat surface, but as shown in Figure 4, PNIPAAm-FPAA-PVDF membrane roughness increases and has many isolated rough spots, which was also found with PNIPAAm grafted PET membrane[36, 37]. The remarkable topography change is attributed to the grafting of PNIPAM chains.

3.2. Temperature Responsive Water Flux through the PNIPAAm-PVDF Membranes

To investigate the pore opening and closing of PNIPAAm functionalized PVDF membrane due to the swelling and shrinking behavior with response to temperature changes, the water permeability of PNIPAAm-PVDF membrane was measured at temperature below and above LCST. The effects of cross-linker amount and monomer amount are investigated in this section.

3.2.1 Theory—According to Hagen–Poiseuille's (HP) equation [20, 30], the fluid flux is dependent on the following factors:

$$J=\frac{NA\pi\Delta P}{8\eta L}\left(\frac{D}{2}\right)^4 \quad (1)$$

Where J is the volume flux (L/m^2/h); N is the membrane pore density; A is the membrane area; D is the pore diameter; is the dynamic viscosity of water, L is the membrane thickness, and ΔP is the transmembrane pressure difference. According to this equation, the flux is inverse proportional to the viscosity, which is also related to temperature. Therefore, to eliminate the temperature effects, reported flux was normalized by:

$$J=\frac{J_T\eta_T}{\eta_{25^\circ C}} \quad (2)$$

Where J_T*and* represents the reported flux and viscosity at temperature T, and 25°c represents the viscosity of water at 25°C.

Assuming a cylindrical pore and uniform polymer distribution throughout the membrane pores, the effective pore size can be calculated from Eq.1 based on the water flux measurement. Then the volume fraction ( ) of the polymer in the membrane is:

$$\varphi=1-(D_f/D_o)^2 \quad (3)$$

Where D_o is the pore diameter for blank membrane; D_f is the pore diameter for functionalized membrane.

3.2.2. Effects of cross-linker amount—In an attempt to control the membrane flux response, the effect of cross-linker amount was investigated. Figure 5 shows the water fluxes of PNIPAAm-PVDF membranes with different cross-linker amounts ranging from 0.1% to 2%. As for comparison, the permeability of blank PVDF membrane is 3809L/m^2/h/bar. When temperature increased, the permeability of blank PVDF membrane was increased to 4864L/m^2/h/bar due to water viscosity decrease (as indicated in Eq.1). To eliminate the effects of viscosity, all the flux data were normalized with viscosity at 25°C. As shown in Figure 5, PNIPAAm-PVDF membranes show obvious thermo-responsive characteristics. The ratio of flux at 30°C (below LCST) and 34°C (above LCST) was plotted in Figure 5 to directly compare the degree of response. For all the cross-linker amounts from 0.1 to 0.5 mol%, an increase in the relative permeability ratio or "valve" ratio was observed reaching a maximum of approximately 15 at the temperature about 34°C (above LCST). The valve mechanism was achieved by the transition between the polymer swelling (30°C) and shrinking (34°C) to close and open the membrane pore[26, 33] (as shown in the SEM image (Figure 3B and 3C)). The constant permeability(J_{30}'/J_{30}=1) when temperature was returned to 30°C, indicates the temperature responsive reversibility and stability. It should be noted that although 0.5mol% cross-linker amount shows the best "valve" ratio, a more stable network are required since there is no covalent bonding between the filled polymer chain and the membrane. 15 times of flux increase may cause the filled polymer chain to be washed out. On the other hand, for cross-linker amounts increased from 0.5 and up to 2.0 mol%, the permeability ratio decreased, but still retained temperature-responsive behavior. At higher crosslinker amount, the lower temperature response is due to the limited movement of PNIPAAm chains immobilized in membrane pores, which can reduce the swelling ratio of hydrogel[30, 37]. In addition for separation application, the system can also be used to immobilize metal nanoparticles to degrade chloro-organics. Too much cross-linking may cause the diffusion problems and reduce the reaction. Therefore, by varying the cross-linker amount, swelling–shrinking ratio of the thermo-sensitive membrane can be modified leading to greater or lesser flow through the membrane pores.

3.2.3. Effects of Monomer Concentration—Since this temperature-dependent permeation is due to the conformation change of PNIPAAm chain on the surface and also in the membrane pores, the response of functionalized PVDF membranes can be regulated by the control of grafting amount of NIPAAm. Figure 6 shows the relationship of flux and NIPAAm concentration. The flux was decreased as the increase of NIPAAm concentration. Wang et al[38] has proved the linear relationship between grafting amount and NIPAAm concentration in the range of 0-15%.Therefore, more pores will be occupied by the polymer with the monomer amount increase, which leads to the reduction of water permeability. According to the Hagen-Poiseuille's law, the mean effective pore diameter was calculated base on Eq. 1 and the result is shown in Figure 6. It shows the effective pore diameter decreased from 230 nm to 100 nm (650 nm for blank PVDF) with the increase of monomer amount from 1 to 5 wt% due to the increase of pore coverage by PNIPAAm hydrogels. By adjusting the monomer concentration, one would expect to control the morphology of the membrane pore and further regulate the temperature responsive behavior. This result is consistent with the previous reports by Lue and Wang's groups[30, 37] and also a further proof of PNIPAAm inside the membrane pores.

3.3. Quantification of Temperature Dependent Unsteady-state Membrane Flux

In order to reveal the dynamics of thermo-responsive gating behavior, the unsteady-state hydraulic flux through the PNIPAAm-PVDF membrane was plotted against controlled step changes in solvent feed temperature as shown in Figure 7. The feed temperature was raised by 4 degrees from 30.0°C to 34.0°C within an interval of 180 seconds. The observed change in steady-state flux was found to occur over a relatively short time interval of approximately 20 minutes. The second run (red circle, Figure 7) shows agreeable reproducibility in absolute flux measurements as well as reversibility of temperature flux response over a similar time interval. The reversible flux response supports the conclusion that the stable network of cross-linked hydrogel and porous PVDF support provides increased mechanical robustness over extended periods of use and higher operating pressures.

3.4 Temperature and pH dependent hydraulic permeability of PNIPAAm-FPAA-PVDFHE membrane

The flux of aqueous solutions through the PNIPAAm-FPAA-PVDFHE Sepro membrane was investigated as functions of both temperature (in the temperature range from 22°C to 45°C) and pH (pH=4, 6.3, 7.3). The water permeability data are plotted against temperature and fitted with error function[20].

$$erf\,(T) = A + B\int_0^T exp\left[-\frac{(T-T_c)^2}{(\Delta T)^2}\right] dT \quad (4)$$

Where A and B are independent constants, T_c is the LCST (°C), and ΔT is the temperature transition change from open-state to closed-state (°C). By using this model, the experimental parameters, such as open-state permeability, close-state permeability, switching temperature, switching range can be determined. The regression was performed through a nonlinear least-squares curve fitting (lsqnonlin) in MATLAB®. The results are shown in Figure 8 and the fitted data are in Table S1. For comparison, the temperature has no effects on the full-scale FPAA-PVDFHE Sepro membrane as shown in the inset of Figure 8. In general, the water flux through the PNIPAAm-FPAA-PVDFHE Sepro membrane is both temperature and pH dependent. The water flux decreases with the increase of water pH from 4 to 7.3 at a fixed temperature. The volume fraction of hydrogel in FPAA-PVDFHE and PNIPAAm-FPAA-PVDFHE membranes are estimated to be 51% and 92% (pH=6.5) respectively, by using Eq. 1 and Eq. 3. The volume fraction can significantly affect the transport of solute through the membrane pores and can be easily optimized by changing the grafting ratio of the hydrogel or using a membrane with different size.

It should be noticed that after the run at pH=7.3, another run with different temperatures at pH=6.3 was conducted (dark red broken circle in Figure 8). The same flux data indicates that the pH and temperature-dependent changes in water flux are completely reversible. The change in flux in response to pH can be caused by the conformation change of acrylic acid polymer chain in the PNIPAAm-FPAA-PVDFHE Sepro membrane. It also shows that at higher temperature, the pH sensitivity is also enhanced. When the temperature is higher than 32°C (above LCST), the water flux exhibits a more marked increase with the pH decreasing

from 7.3 to 4 (Figure 8). This may because the PNIPAAm polymer collapses and becomes hydrophobic at temperature above LCST. More ionized carboxylate groups at higher temperature[39], allows the enhanced interaction between PAA chains and water[40]. As a consequence, pH sensitivity at higher temperature is increased. Furthermore, the temperature sensitivity increases in the lower pH range. As shown in Figure 8, the flux showed more obvious change at pH=4 than pH=7.3. This phenomenon can be explained that the PNIPAAm chain will play an predominant role when the PAA polymer chain exhibit a helical conformation at lower pH[41-43]. More PNIPAAm chain will interact with water leading to a higher temperature sensitivity.

Furthermore, as documented, the PNIPAAm-PAA copolymers can shift the LCST to higher temperature, or even worse, can cause the loss of temperature responsivity at higher pH value[44]. However, in this work, the results (Figure 8 and Table S1) shows pH and temperature response are independent and the pH values has negligible effect on LCST. This may because PNIPAAm and PAA are chemically independent with the formed interpenetrating network (IPN)[45] by post polymerization of NIPAAm (cross-linked) within the cross-linked PAA gel network. It also offers more favorable mechanical properties when compared with individual cross-linked network[46]. Therefore, it can broaden the system to very sensitive application, such as, drug delivery. Also, the alterable water flux can be utilized as a sensor and valve to control the liquid transfer process by temperature response.

Since the polymer was not covalently bonded with the membrane, a natural question might be raised about the stability of the membrane. Firstly, the reversible temperature and pH responsive properties can be cycled repeatedly as shown in Figure 7 and Figure 8. Secondly, to check the long term stability of the membrane, the water flux and responsive properties of a same membrane sample were tested over two experimental periods which were 6 months apart. The membrane was washed with DIUF, dried under vacuum and stored in a sample bag. The water flux slightly decreases from 14 $L/m^2/h$ to 12 $L/m^2/h$ at pH=6.3 and T=23°C during the 6 months time interval. In addition, the temperature responsive on-off ratio was reduced from 6.8 to 6.4 calculated from the ratios of permeability at 40°C to that of 25°C at pH 6.3. The on-off ratio also slightly decreased from 4.6 to 4.3 for pH 4 to pH 7 at T=25°C. These data confirm the stability of the responsive membranes and the promising potential in controlled separation or drug release applications.

3.5 Dextran Rejection through PNIPAAm-PVDF *Membranes*

The dramatic change of pore size of the thermo-sensitive membranes makes it possible to separate molecules with different size. To evaluate the temperature effect on the separation behavior, dextran was utilized and the rejections with respect to temperature are shown in Figure 9 and Figure 10. The dextran molecular weight is 2,000,000 g/mol and the feed concentration is 2 g/L. For both PNIPAAm-PVDF (Millipore) and PNIPAAm-FPAA-PVDFHE (Sepro) membranes, the flux of solution increases, while the dextran rejection decreases with the increasing of temperature. The reduction of rejection can be explained by the pore size increasing, which leads to more molecules transport through the pore at higher temperature. To further prove the rejection results, GPC experiment was conducted to

evaluate the dextran concentration before and after the dextran permeation and the result is shown in Figure S4. PNIPAAm-PVDF Millipore membrane (5% NIPAAm with 5% cross-linker) (Figure 9) was used as an example and the result shows that as expected, at lower temperature with higher rejection (almost 100%), the dextran concentration in the permeate is almost 0, which is consistent with that of TOC results.

The monomer concentration effect on the dextran rejection was also investigated as shown in Figure 9. The dextran rejection is obviously increased from 5% to 95% (30°C) with the monomer concentration increasing from 1% to 5%. The pH effect on the dextran rejection through PNIPAAm-FPAA-PVDFHE Sepro membrane was also investigated as shown in Figure 10. It indicates that at constant temperature, the dextran rejection increase with the increase of pH from 4 to 7.3. This result is in good agreement with the swelling and shrinking of PAA chain in membrane pores. At pH 7.3 above pKa (~4.5), the PAA chain swells and reduces the pore size which subsequently decrease the pore size of the membrane and increase the mass transfer resistance, resulting the high dextran rejection. For better comparison, the dextran rejection through full-scale FPAA-PVDFHE Sepro membrane at different pH was also studied, which shows no rejection at pH=4 and 6.3, and only 9% rejection at pH=7.3. The confirms that the significant increase of dextran rejection through PNIPAAm-FPAA-PVDFHE Sepro membrane is due to the formed PNIPAAm chains in the membrane.

3.6 Na_2SO_4 Rejection through PNIPAAm-FPAA-PVDFHE Sepro Membranes

To further illustrate temperature effects on the nanofiltration type separation properties, single salt rejection studies were performed using 100 mg/L and 1000 mg/L Na_2SO_4 at different temperatures as shown in Figure 11. The salt rejection is based on both steric exclusion and donnan exclusion. Therefore, Na_2SO_4 rejection through full-scale FPAA-PVDFHE Sepro membrane was firstly studied as a control experiment to eliminate the charge effect by PAA. The result shows 12.2% rejection at 25°C, 11.5% at 30°C and 5.3% at 34°C at pH=6.5, which is attributed to to the high salt diffusion through the membrane at higher temperature [47]. On the other hand, for PNIPAAm-FPAA-PVDFHE Sepro membrane, the rejection increased to 32% at temperature below LCST and 25% at temperature above LCST because of the more dominated steric exclusion than donnan exclusion. It should be noted that the increase of the salt concentration from 100 mg/L to 1000 mg/L reduces the Na_2SO_4 rejection from 30% to 5% (25°C), which is reasonable because as the salt concentration increases, the electrostatic repulsion between polymer chains reduces, so the interaction between salt and membrane decreases leading to the less rejection of salt[47]. These results will be more important because this separation properties through polymer filled membrane can be switched from molecules selective from ultra-filtration to micro-filtration or even just filtration (transport of all molecules) through only the temperature and pH change.

3.6 Catalytic Dechlorination

In our previous publication[48], PNIPAAm-PAA hydrogel has been used as support to immobilized nanoparticles and used in the degradation of toxic chloro-organics with improved reactivity by the temperature responsive polymer. In this work, the hydrogel was

filled within the membrane to increase the mechanical strength and can be used under convective flow to reduce the mass transfer resistance. Another advantage is that the nanoparticles amount in the membrane pore can be controlled. As shown in Figure S5, after 3 runs, the iron loading amount is increased to about 15 mg. The corresponding flux is also shown in Figure S5. With the increase of nanoparticles amount in the membrane, more membrane pores are occupied, causing the reduction of flux. Since the nanoparticles are formed by iron exchange followed by reduction, the free –COOH groups from PAA can also be utilized to capture ferrous ion again. Therefore, the iron loading amount can keep increasing. However this will sacrifice the effective membrane pore size, which in turn requires high pressure for the reaction. By adjusting the iron loading amount, the optimized reaction reactivity can be obtained.

The nanoparticles were studied for the degradation of trichloroethylene (TCE), an ubiquitous pollutant. The detailed information about using Fe or Fe/Pd nanoparticle for dechlorination can be found in our publications[22, 23, 49]. Pd is used to catalyze the reaction. The reactivity can be calculated by the pseudo-first order model[50, 51]:

$$\frac{dC}{dt} = -k_{SA}\alpha_s\rho_m C \quad (5)$$

Where, C is TCE concentration in water (mg/L); k_{SA} is surface area normalized reactivity(L/m^{2}h); α_s is the specific surface area of nanoparticles (m^2/g); ρ_m is the mass concentration of nanoparticles (g/L), t is the time (h).

Figure 12 shows the successful degradation of TCE by Fe/Pd nanoparticles (50 nm size as shown in the inset SEM image) with 70% of TCE degradation and 90% of chloride formation as the product within 3 h. The surface area normalized reactivity was calculated to be 0.15 L/m^2/h by using Eq. 5., which is consistent with reported dechlorination reactivity by Fe/Pd nanoparticles[49, 51, 52]. Our previous study shows three times increase of reactivity by using Fe/Pd nanoparticles immobilized in PNIPAAm-PAA hydrogel [48]. Our future work will involve the effect of temperature on reactivity by Fe/Pd nanoparticles within temperature responsive PNIPAAm-FPAA-PVDF membrane. Furthermore, the cooperative work for full-scale membrane manufacturing will continue to optimize the membranes for direct reactive nanoparticles synthesis. For the first time, direct in-situ synthesis of NPs in the full-scale membranes is conducted and thus will enhance the application for on-site groundwater treatment.

5. Conclusion

In this study, temperature responsive PNIPAAm-PVDF and both pH and temperature PAA-PNIPAAm-PVDF membranes prepared by pore-filling method with wide range of both monomer concentration and cross-linker were investigated systematically. A rapid and reversible swelling and shrinking of PNIPAAm chains can enlarge and reduce the effective pore size of the membrane. The water flux through the temperature responsive membrane varied by up to15 times for temperature changes from 30 °C(below LCST) to 34 °C (above LCST). The system can be employed as a sensor or a valve with temperature response.

Dextran solution was used to evaluate the separation properties by this temperature responsive membrane and the result showed dramatic separation performance change by temperature change. To our knowledge, full-scale pore functionalization of PVDF microfiltration membranes to obtain responsive behavior has not been reported in the literature. Direct synthesis of catalytic metal nanoparticles with various loading amounts was established for toxic chloro-organics degradation. This functionalized membrane with tunable size-selectivity and temperature-responsive features can advance the separation process.

Supplementary Material

Refer to Web version on PubMed Central for supplementary material.

Acknowledgments

This research was supported by National Institute of Environmental Health Sciences Superfund Research Program (NIEHS-SRP) and by the US Department of Energy (DOE) KRCEE programs. Austin Isner was in our NSF/REU program, Krysta Waldrop, and Anthony Saad (MIT, Chemical Engineering Student) were undergraduate researchers. The authors acknowledge Sepro Membrane, Inc., Oceanside, CA for the joint development work on the PVDF functionalized membranes.

References

1. Alexander C. Stimuli-responsive hydrogels: Drugs take control. Nat Mater. 2008; 7:767–768. [PubMed: 18813300]
2. Stuart MAC, Huck WTS, Genzer J, Muller M, Ober C, Stamm M, Sukhorukov GB, Szleifer I, Tsukruk VV, Urban M, Winnik F, Zauscher S, Luzinov I, Minko S. Emerging applications of stimuli-responsive polymer materials. Nat Mater. 2010; 9:101–113. [PubMed: 20094081]
3. Sieradzki K. Potential Solutions for Creating Responsive Materials. Science. 2011; 332:1158–1159. [PubMed: 21636763]
4. Pérez RA, Won J-E, Knowles JC, Kim H-W. Naturally and synthetic smart composite biomaterials for tissue regeneration. Adv. Drug Del. Rev. 2013; 65:471–496.
5. Chan A, Orme RP, Fricker RA, Roach P. Remote and local control of stimuli responsive materials for therapeutic applications. Adv. Drug Del. Rev. 2013; 65:497–514.
6. Kobayashi, J.; Akiyama, Y.; Yamato, M.; Okano, T. 5.06 - Biomaterials: Temperature-Responsive Polymer. In: Murray, M-Y., Editor-in-Chief, editor. Comprehensive Biotechnology. Second Edition. Academic Press; Burlington: 2011. p. 51-64.
7. Fleige E, Quadir MA, Haag R. Stimuli-responsive polymeric nanocarriers for the controlled transport of active compounds: Concepts and applications. Adv. Drug Del. Rev. 2012; 64:866–884.
8. Ying L, Wang P, Kang ET, Neoh KG. Synthesis and Characterization of Poly(acrylic acid)-graft-poly(vinylidene fluoride) Copolymers and pH-Sensitive Membranes. Macromolecules. 2001; 35:673–679.
9. Çakmak S, Çakmak AS, Gümü derelio lu M. PNIPAAm-grafted thermoresponsive microcarriers: Surface-initiated ATRP synthesis and characterization. Materials Science and Engineering. 2013; C(33):3033–3040. [PubMed: 23623129]
10. Costa E, Lloyd MM, Chopko C, Aguiar-Ricardo A, Hammond PT. Tuning Smart Microgel Swelling and Responsive Behavior through Strong and Weak Polyelectrolyte Pair Assembly. Langmuir. 2012; 28:10082–10090. [PubMed: 22676290]
11. Du H, Wickramasinghe R, Qian X. Effects of Salt on the Lower Critical Solution Temperature of Poly (N-Isopropylacrylamide). J. Phys. Chem. B. 2010; 114:16594–16604. [PubMed: 21090725]
12. Zhang Y, Chan HF, Leong KW. Advanced materials and processing for drug delivery: The past and the future. Adv. Drug Del. Rev. 2013; 65:104–120.

13. Fan Q, Sirkar KK, Wu J. A thermo-sensitive release system based on polymeric membrane for transdermal delivery of doxycycline HCl. J. Membr. Sci. 2009; 337:175–181.
14. Hu J, Liu S. Responsive Polymers for Detection and Sensing Applications: Current Status and Future Developments. Macromolecules. 2010; 43:8315–8330.
15. Roy D, Cambre JN, Sumerlin BS. Future perspectives and recent advances in stimuli-responsive materials. Prog. Polym. Sci. 2010; 35:278–301.
16. Wandera D, Wickramasinghe SR, Husson SM. Stimuli-responsive membranes. J. Membr. Sci. 2010; 357:6–35.
17. Huang J, Wang X-L, Qi W-S, Yu X-H. Temperature sensitivity and electrokinetic behavior of a N-isopropylacrylamide grafted microporous polyethylene membrane. Desalination. 2002; 146:345–351.
18. Liang L, Shi M, Viswanathan VV, Peurrung LM, Young JS. Temperature-sensitive polypropylene membranes prepared by plasma polymerization. J. Membr. Sci. 2000; 177:97–108.
19. Shtanko NI, Kabanov VY, Apel PY, Yoshida M, Vilenskii AI. Preparation of permeability-controlled track membranes on the basis of ‘smart’ polymers. J. Membr. Sci. 2000; 179:155–161.
20. Lue SJ, Chen C-H, Shih C-M, Tsai M-C, Kuo C-Y, Lai J-Y. Grafting of poly(N-isopropylacrylamide-co-acrylic acid) on micro-porous polycarbonate films: Regulating lower critical solution temperatures for drug controlled release. J. Membr. Sci. 2011; 379:330–340.
21. Tan X, Tan SP, Teo WK, Li K. Polyvinylidene fluoride (PVDF) hollow fibre membranes for ammonia removal from water. J. Membr. Sci. 2006; 271:59–68.
22. Smuleac V, Bachas L, Bhattacharyya D. Aqueous-phase synthesis of PAA in PVDF membrane pores for nanoparticle synthesis and dichlorobiphenyl degradation. J. Membr. Sci. 2010; 346:310–317.
23. Lewis SR, Datta S, Gui M, Coker EL, Huggins FE, Daunert S, Bachas L, Bhattacharyya D. Reactive nanostructured membranes for water purification. Proceedings of the National Academy of Sciences. 2011; 108:8577–8582.
24. Li Y, Chu L-Y, Zhu J-H, Wang H-D, Xia S-L, Chen W-M. Thermoresponsive Gating Characteristics of Poly(N-isopropylacrylamide)-Grafted Porous Poly(vinylidene fluoride) Membranes. Industrial & Engineering Chemistry Research. 2004; 43:2643–2649.
25. Choi Y-J, Yamaguchi T, Nakao S.-i. A Novel Separation System Using Porous Thermosensitive Membranes. Industrial & Engineering Chemistry Research. 2000; 39:2491–2495.
26. Yu J-Z, Zhu L-P, Zhu B-K, Xu Y-Y. Poly(N-isopropylacrylamide) grafted poly(vinylidene fluoride) copolymers for temperature-sensitive membranes. J. Membr. Sci. 2011; 366:176–183.
27. Chen Z, Cui Z-M, Cao C-Y, He W-D, Jiang L, Song W-G. Temperature-Responsive Smart Nanoreactors: Poly(N-isopropylacrylamide)-Coated Au@Mesoporous-SiO2 Hollow Nanospheres. Langmuir. 2012; 28:13452–13458. [PubMed: 22909224]
28. Susanto H, Ulbricht M. Photografted Thin Polymer Hydrogel Layers on PES Ultrafiltration Membranes: Characterization, Stability, and Influence on Separation Performance. Langmuir. 2007; 23:7818–7830. [PubMed: 17547431]
29. Gui M, Ormsbee LE, Bhattacharyya D. Reactive Functionalized Membranes for Polychlorinated Biphenyl Degradation. Industrial & Engineering Chemistry Research. 2013; 52:10430–10440.
30. Lue SJ, Hsu J-J, Chen C-H, Chen B-C. Thermally on–off switching membranes of poly(N-isopropylacrylamide) immobilized in track-etched polycarbonate films. J. Membr. Sci. 2007; 301:142–150.
31. Rzaev ZMO, Dinçer S, Piskin E. Functional copolymers of N-isopropylacrylamide for bioengineering applications. Prog. Polym. Sci. 2007; 32:534–595.
32. Ying L, Yu WH, Kang ET, Neoh KG. Functional and Surface-Active Membranes from Poly(vinylidene fluoride)-graft-Poly(acrylic acid) Prepared via RAFT-Mediated Graft Copolymerization. Langmuir. 2004; 20:6032–6040. [PubMed: 16459627]
33. Ying L, Kang ET, Neoh KG. Synthesis and Characterization of Poly(N-isopropylacrylamide)-graft-Poly(vinylidene fluoride) Copolymers and Temperature-Sensitive Membranes. Langmuir. 2002; 18:6416–6423.
34. Cheng Z, Zhu X, Kang ET, Neoh KG. Modification of Poly(ether imide) Membranes via Surface-Initiated Atom Transfer Radical Polymerization. Macromolecules. 2006; 39:1660–1663.

35. Russell TP. Surface-Responsive Materials. Science. 2002; 297:964–967. [PubMed: 12169722]
36. Curti PS, De Moura MR, Radovanovic E, Rubira AF, Muniz EC, Moliterno RA. Surface modification of polystyrene and poly(ethylene terephtalate) by grafting poly(N-isopropylacrylamide). J Mater Sci Mater Med. 2002; 13:1175–1180. [PubMed: 15348662]
37. Xiaoling W, Marian GM. Grafting of poly(N isopropylacrylamide) onto nylon and polystyrene surfaces by atmospheric plasma treatment followed with free radical graft copolymerization. J. Appl. Polym. Sci. 2007; 104:3614–3621.
38. Wang X-L, Huang J, Chen X-Z, Yu X-H. Graft polymerization of N-isopropylacrylamide into a microporous polyethylene membrane by the plasma method: technique and morphology. Desalination. 2002; 146:337–343.
39. Reijenga JC, Gagliardi LG, Kenndler E. Temperature dependence of acidity constants, a tool to affect separation selectivity in capillary electrophoresis. J. Chromatogr. A. 2007; 1155:142–145. [PubMed: 17046005]
40. Ying L, Kang ET, Neoh KG. Characterization of membranes prepared from blends of poly(acrylic acid)-graft-poly(vinylidene fluoride) with poly(N-isopropylacrylamide) and their temperature- and pH-sensitive microfiltration. J. Membr. Sci. 2003; 224:93–106.
41. Debord JD, Lyon LA. Synthesis and Characterization of pH-Responsive Copolymer Microgels with Tunable Volume Phase Transition Temperatures. Langmuir. 2003; 19:7662–7664.
42. Chen Y-C, Xie R, Chu L-Y. Stimuli-responsive gating membranes responding to temperature, pH, salt concentration and anion species. J. Membr. Sci. 2013; 442:206–215.
43. Shim JK, Lee YB, Lee YM. pH-dependent permeation through polysulfone ultrafiltration membranes prepared by ultraviolet polymerization technique. J. Appl. Polym. Sci. 1999; 74:75–82.
44. Jones CD, Lyon LA. Dependence of Shell Thickness on Core Compression in Acrylic Acid Modified Poly(N-isopropylacrylamide) Core/Shell Microgels. Langmuir. 2003; 19:4544–4547.
45. Xing Z, Wang C, Yan J, Zhang L, Li L, Zha L. pH/temperature dual stimuli-responsive microcapsules with interpenetrating polymer network structure. Colloid. Polym. Sci. 2010; 288:1723–1729.
46. Adem E, Burillo G, Bucio E, Magaña C, Avalos-Borja M. Characterization of interpenetrating networks of acrylic acid (AAc) and N-isopropylacrylamide (NIPAAm) synthesized by ionizing radiation. Radiat. Phys. Chem. 2009; 78:549–552.
47. Wong MCY, Martinez K, Ramon GZ, Hoek EMV. Impacts of operating conditions and solution chemistry on osmotic membrane structure and performance. Desalination. 2012; 287:340–349.
48. Xiao L, Isner AB, Hilt JZ, Bhattacharyya D. Temperature responsive hydrogel with reactive nanoparticles. J. Appl. Polym. Sci. 2013; 128:1804–1814.
49. Xu J, Bhattacharyya D. Fe/Pd Nanoparticle Immobilization in Microfiltration Membrane Pores: Synthesis, Characterization, and Application in the Dechlorination of Polychlorinated Biphenyls. Industrial & Engineering Chemistry Research. 2006; 46:2348–2359.
50. Matheson LJ, Tratnyek PG. Reductive Dehalogenation of Chlorinated Methanes by Iron Metal. Environ. Sci. Technol. 1994; 28:2045–2053. [PubMed: 22191743]
51. Lien H-L, Zhang W.-x. Nanoscale iron particles for complete reduction of chlorinated ethenes. Colloids Surf. Physicochem. Eng. Aspects. 2001; 191:97–105.
52. He F, Zhao D, Liu J, Roberts CB. Stabilization of Fe Pd Nanoparticles with Sodium Carboxymethyl Cellulose for Enhanced Transport and Dechlorination of Trichloroethylene in Soil and Groundwater. Industrial & Engineering Chemistry Research. 2006; 46:29–34.

Research Highlights

- Developed a new approach to create both temperature and pH responsive membranes
- Successfully demonstrated rapid and reversible water permeability
- Tunable and controllable separation with temperature
- In-situ synthesis of catalytic metal nanoparticles in functionalized membranes
- Development of full-scale membrane proved the feasibility of bench-scale results

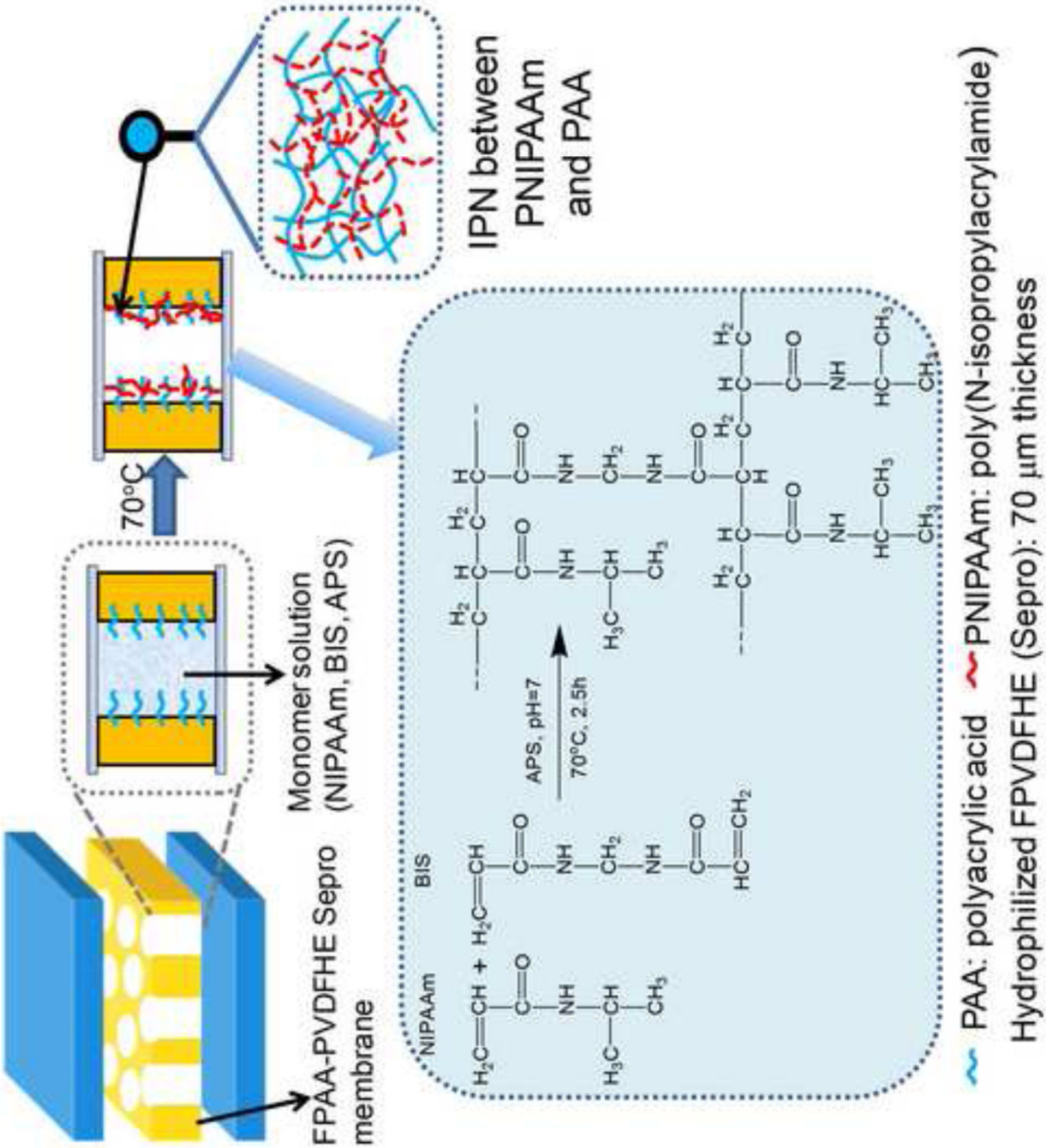

Figure 1.

Schematic of proposed interpenetrating network (IPN) formation by post PNIPAAm functionalization of full-scale cross-linked FPAA-PVDFHE sepro membrane (PNIPAAm-FPAA-PVDFHE).

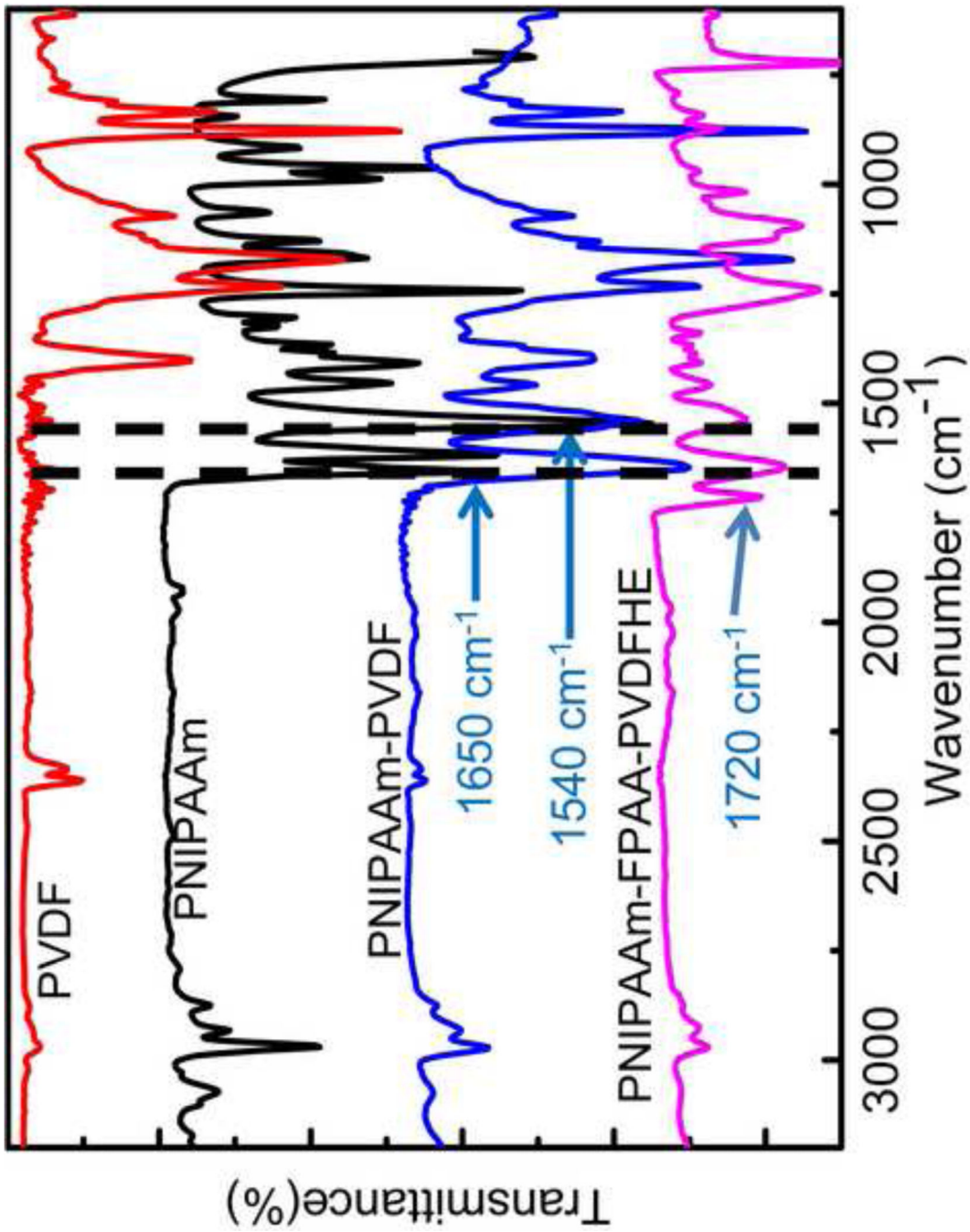

Figure 2.

ATR-FTIR spectrum of blank PVDF, PNIPAAm functionalized PVDF Millipore membrane and PNIPAAm-FPAA-PVDFHE Sepro membrane.

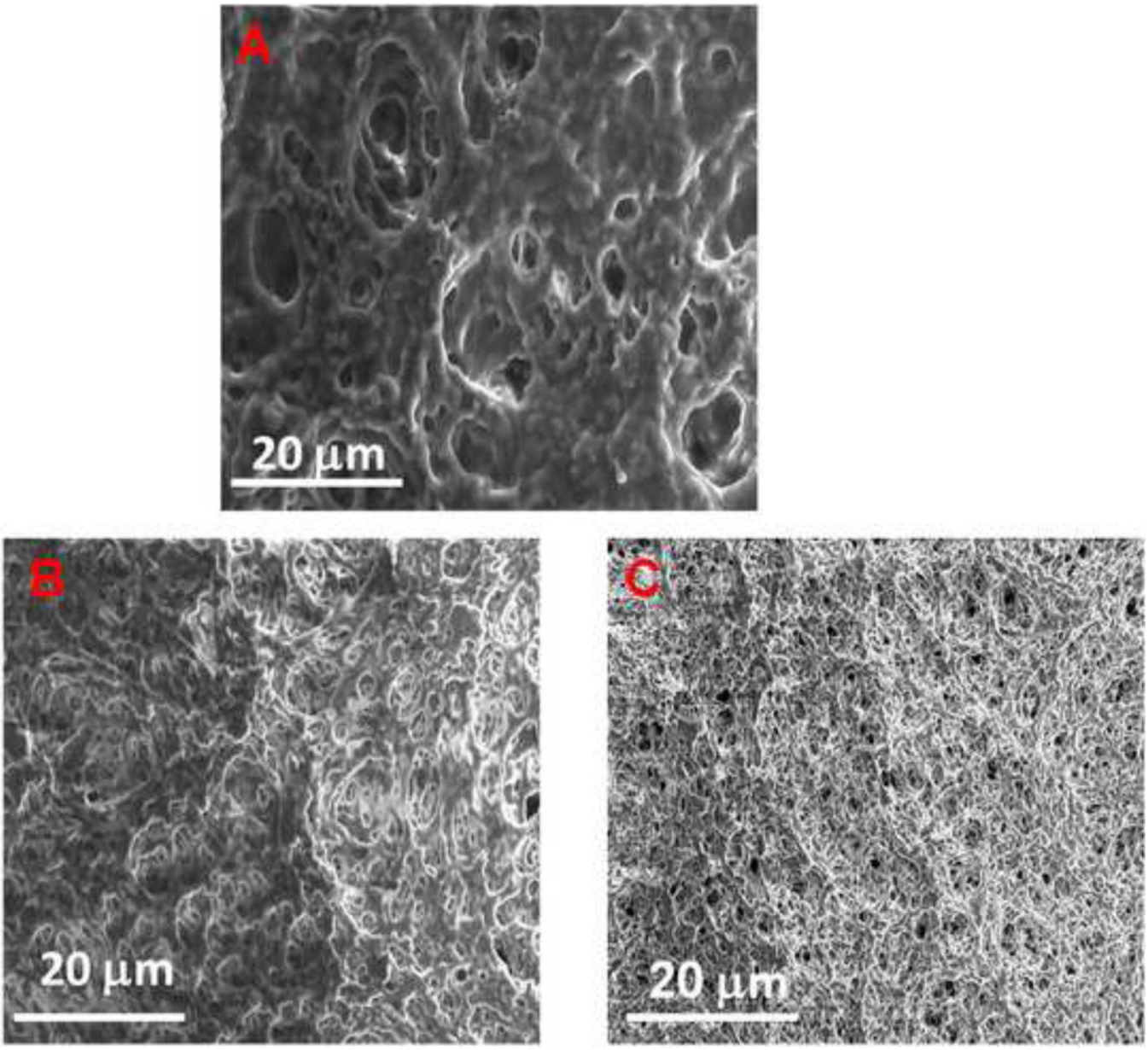

Figure 3.
SEM images of blank PVDF (A) and PNIPAAm-PVDF Millipore membranes (B: 25°C(below LCST); C: 40 °C (above LCST))

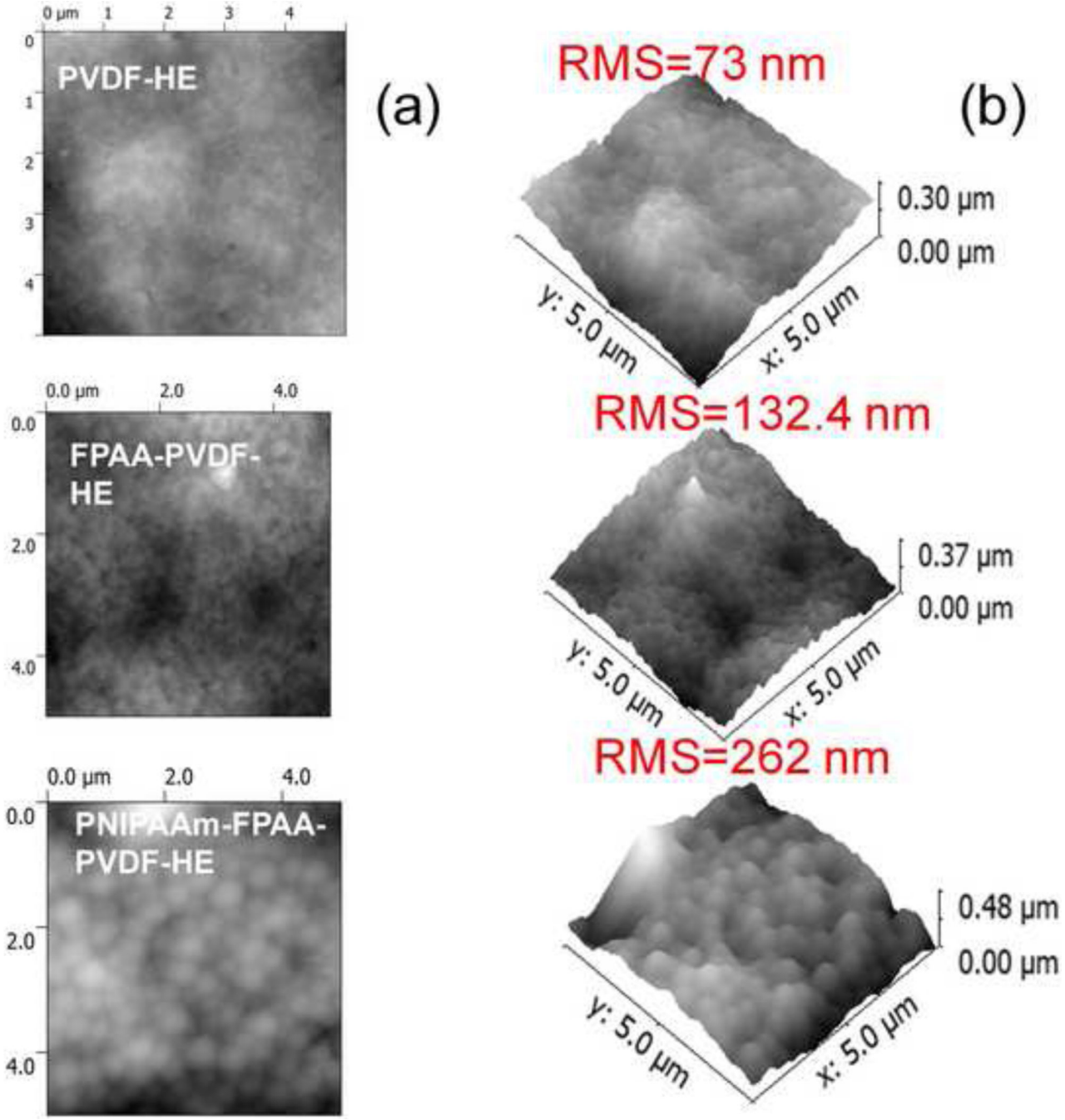

Figure 4.

AFM image blank full-scale PVDFHE Sepro membrane, functionalized FPAA-PVDFHE membrane, PNIPAAm-FPAA-PVDFHE Sepro membrane: (a) top view and (b) 3D.

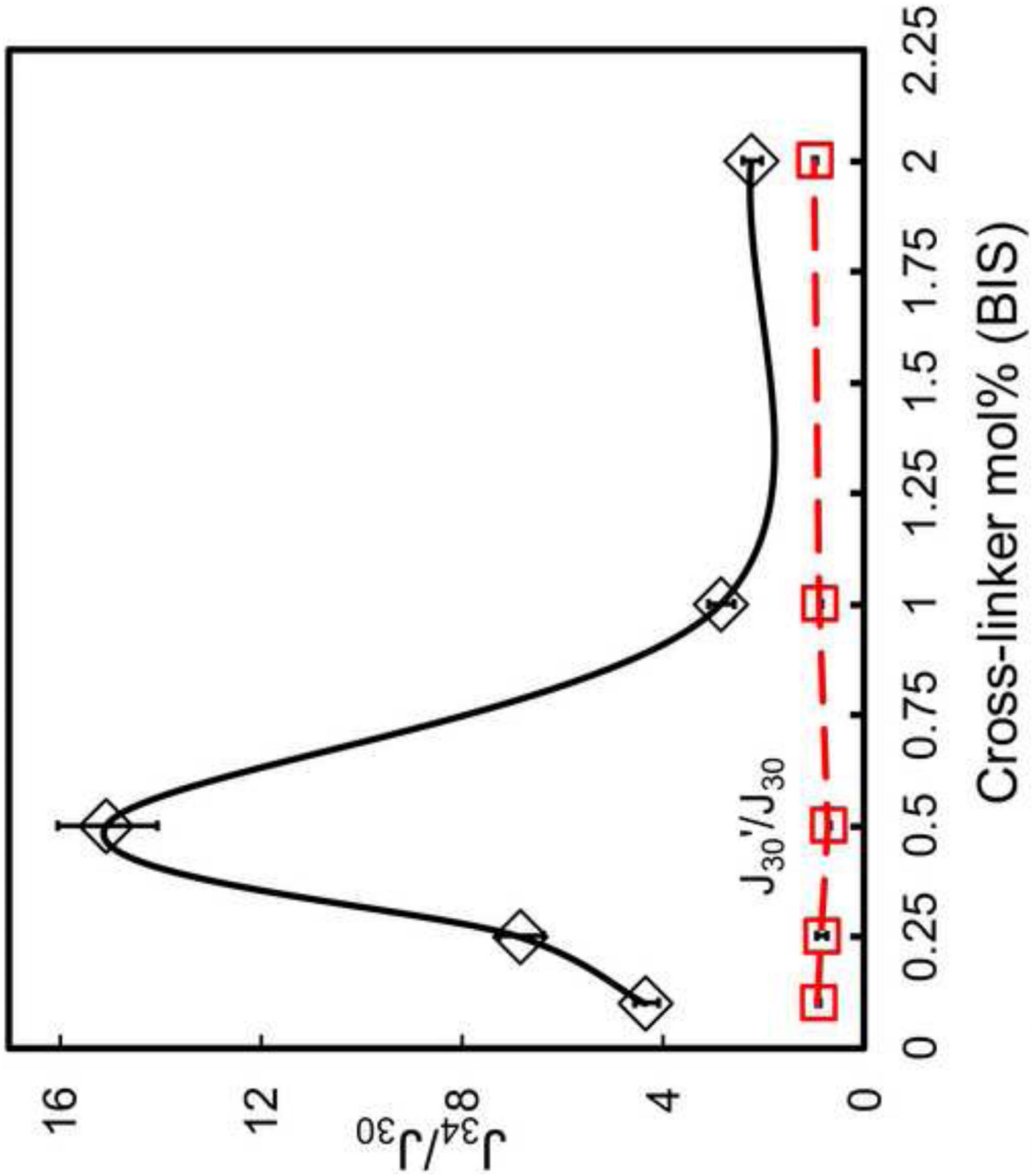

Figure 5.

Dependence of thermally on-off ratio on the cross-linker amounts in the range from 0.1-2.0 mol% in for PNIPAAm-PVDF Millipore membrane (P=1.4 bar). For all the membranes, the NIPAAm concentration for polymerization solution was 5 wt%. Data was corrected with viscosity and normalized by permeability at 30°C.

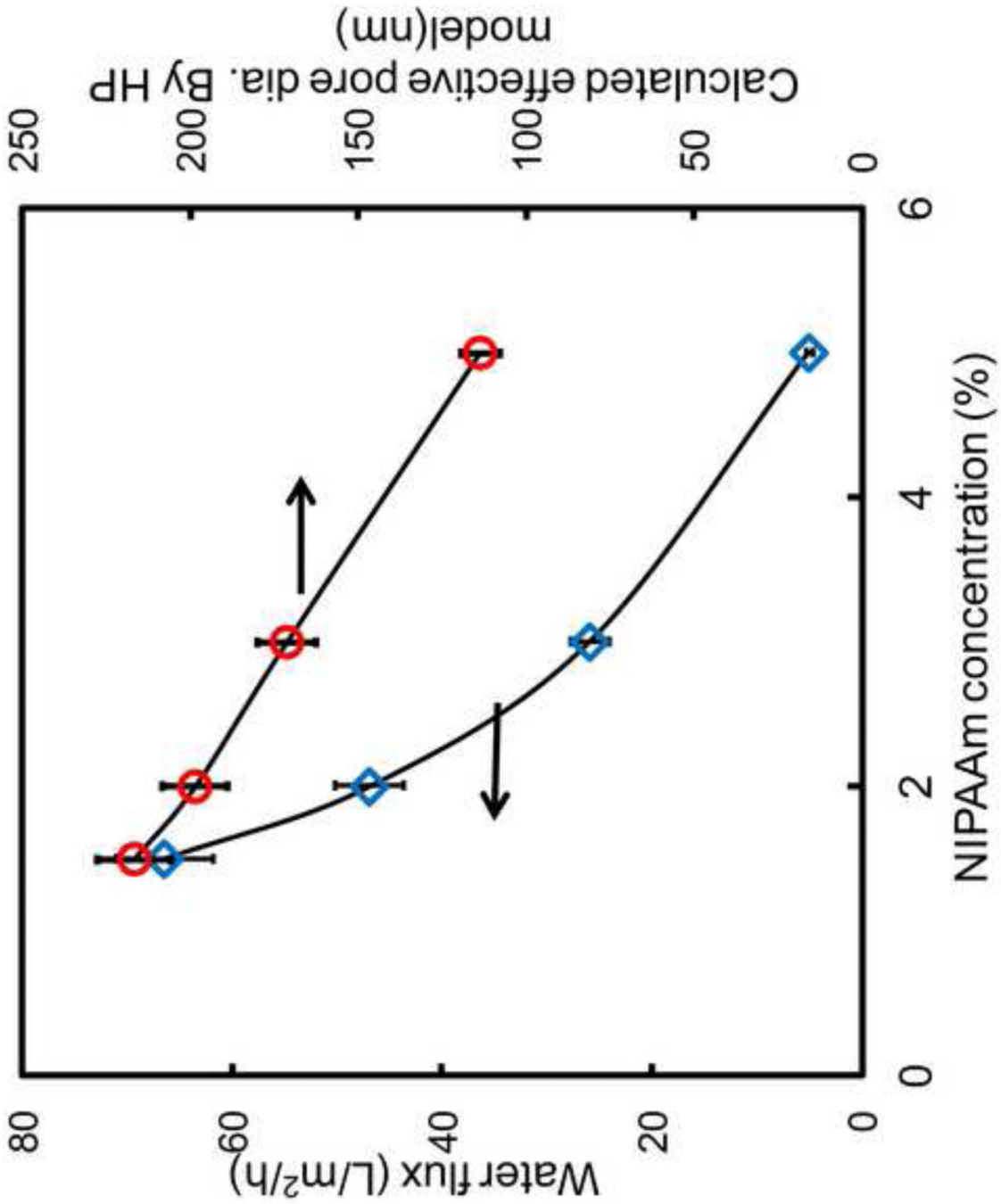

Figure 6.

Effect of monomer (NIPAAm) concentration on water flux at 1.4 bar and calculated effective pore size for PNIPAAm-PVDF Millipore membrane. cross-linker concentration = 1mol%.

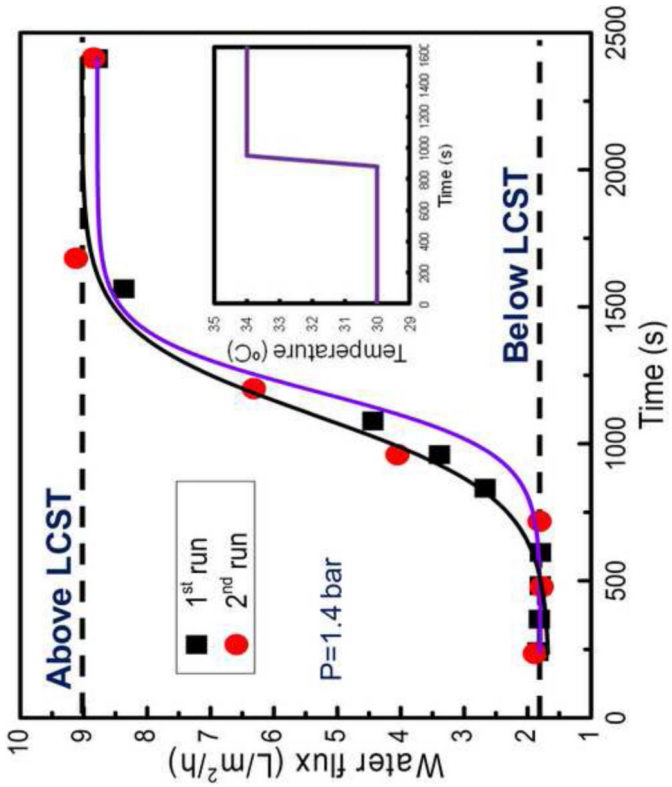

Figure 7.

Dynamic and Reversible flux response versus ramp change in feed temperature above LCST and below LCST through PNIPAAm-PVDF Millipore membrane at P = 1.4 bar. The inset is the experimental temperature step change approximation. For the polymerization, the NIPAAm concentration was 5 wt%, cross-linker was 0.1mol%.

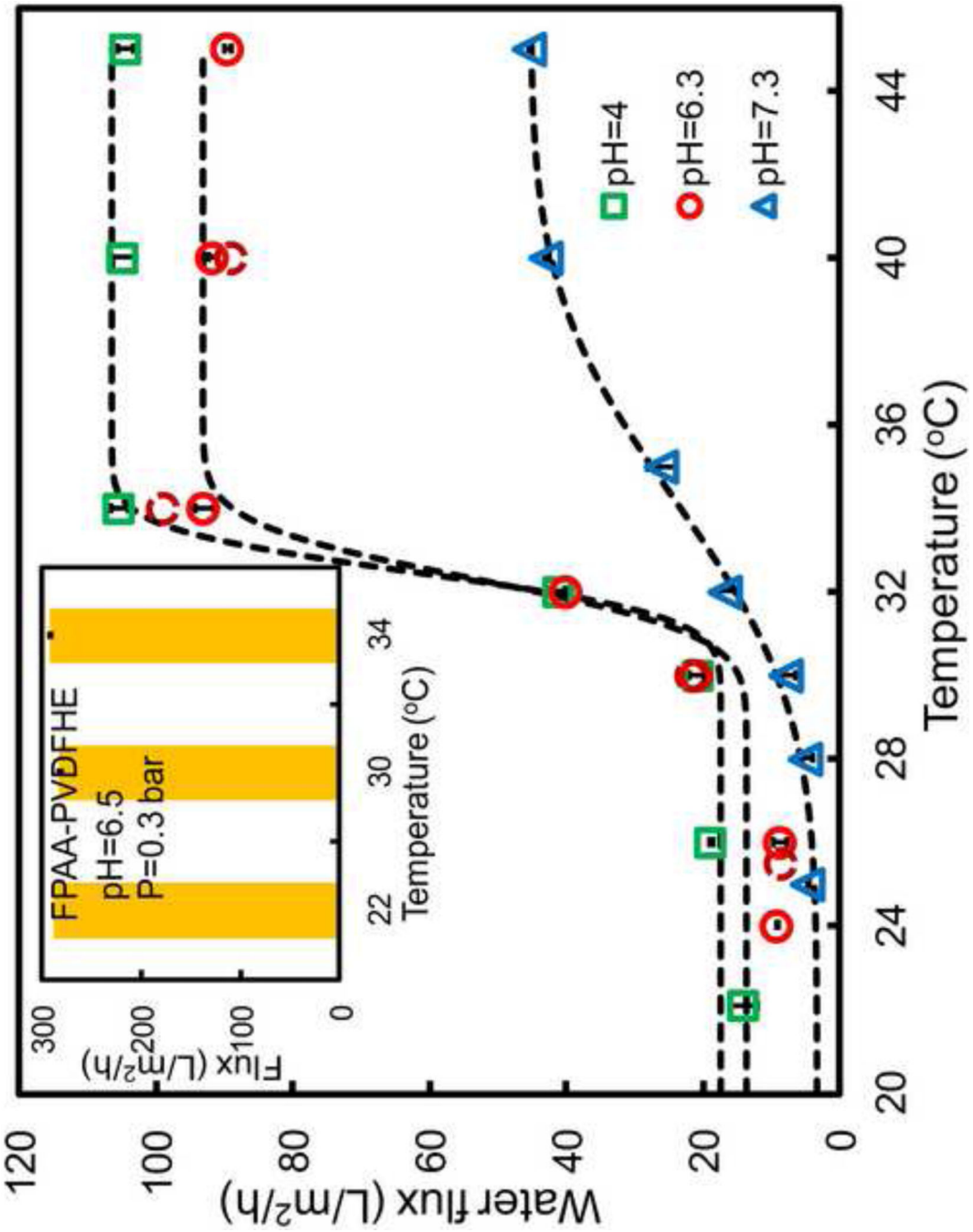

Figure 8.

Temperature and pH effects on the pure water flux at 3.8 bar through PNIPAAm-FPAA-PVDFHE Sepro membrane. For the polymerization, the NIPAAm concentration was 13 wt %, cross-linker was 1mol%. The inset is the temperature effect on the full-scale FPAA-PVDFHE Sepro membrane (pH=6.5, P=0.3 bar). All the flux Data were corrected with viscosity. Data are fitted by error function. Dark red broken circles represent the flux data obtained with different temperature at pH=6.3 after the run at pH=7.3.

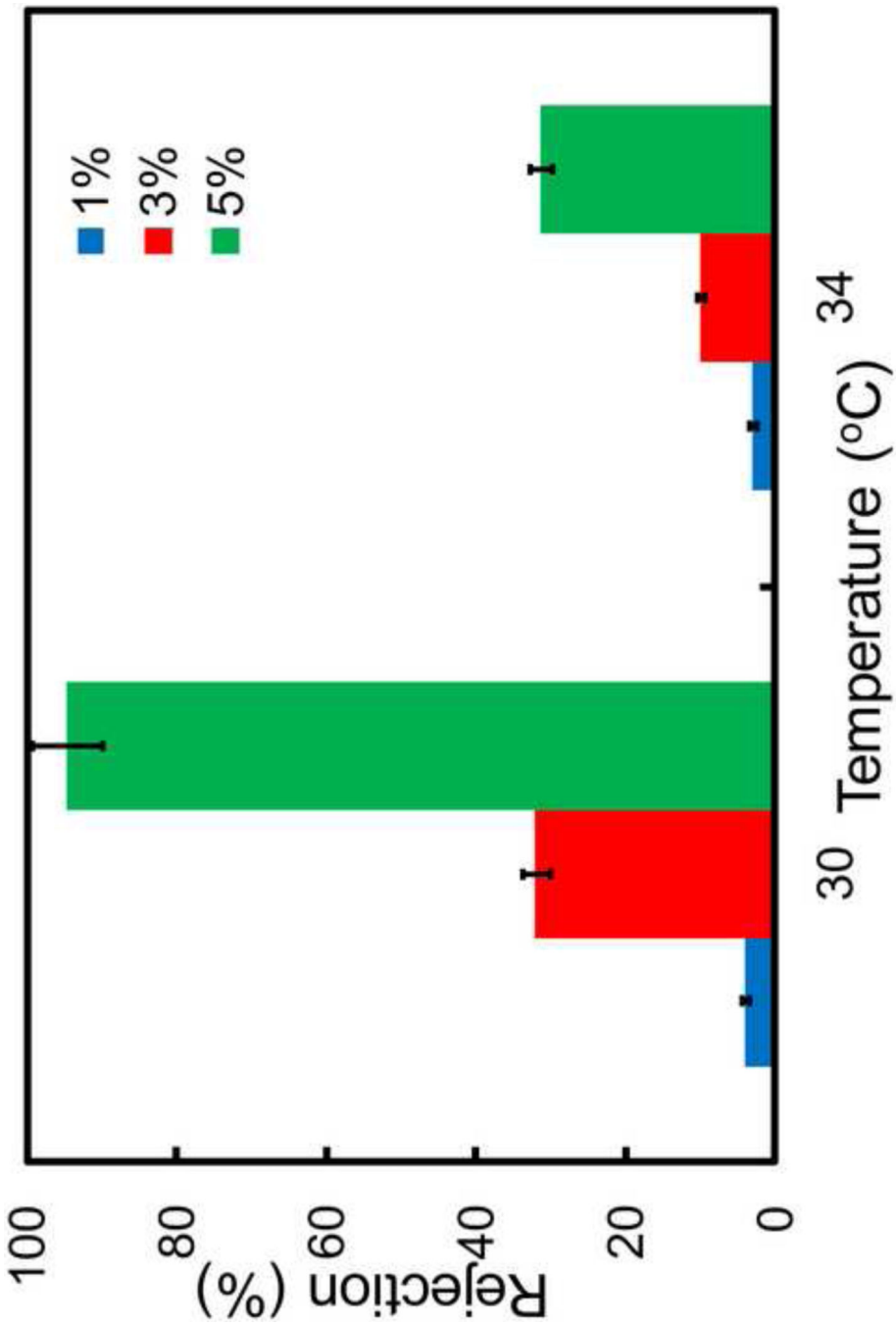

Figure 9.

The effects of temperature and monomer concentration on dextran rejection with PNIPAAm-PVDF Millipore membrane (5mol% cross-linker) (Mw=2,000,000 g/mol; Stokes radius r_s= 26.1nm, calculated from $r_s=0.27 \cdot M_w^{0.498}$).

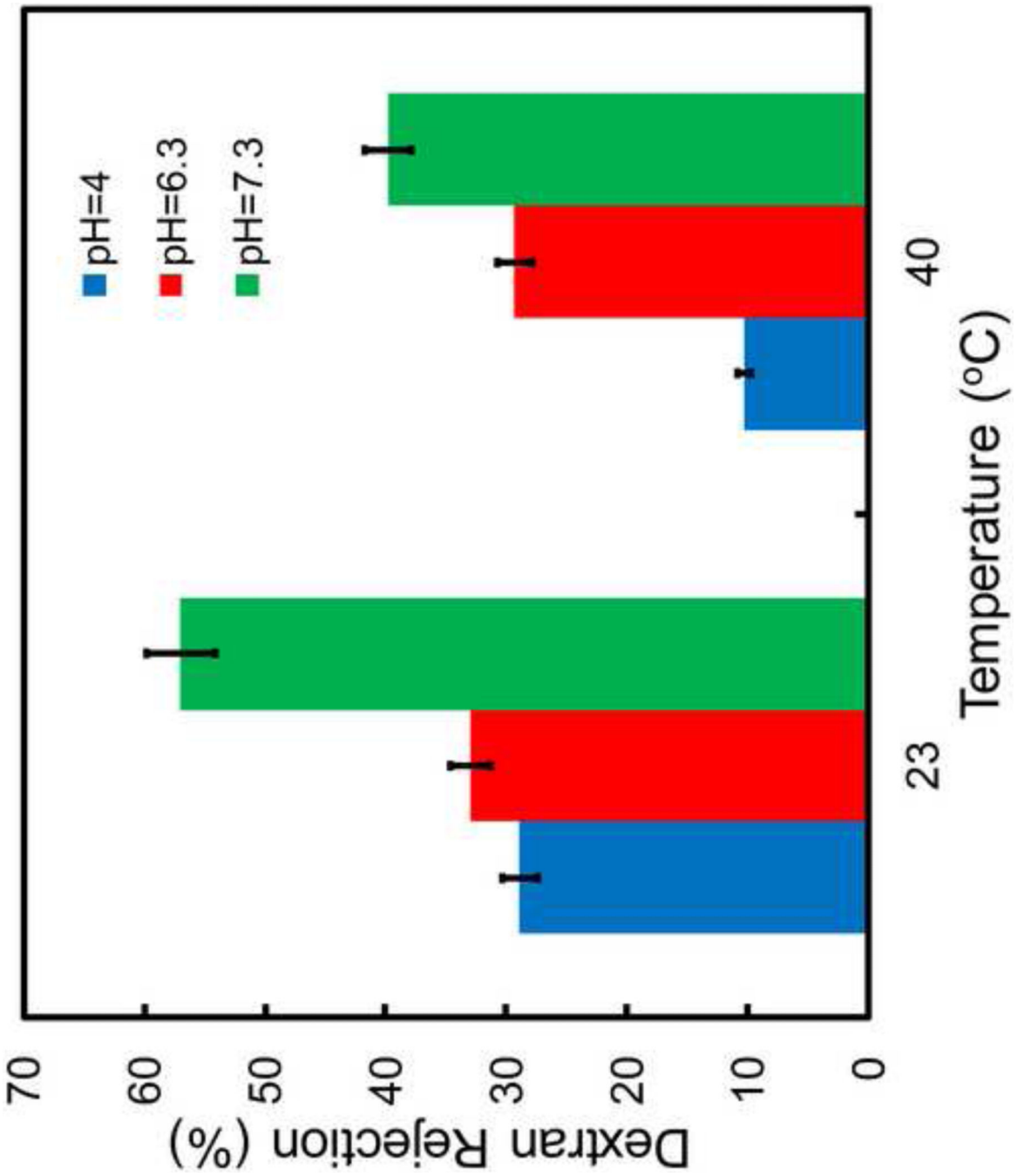

Figure 10.

The effects of temperature and pH on dextran rejection of PNIPAAm-FPAA-PVDF Sepro membrane (M_w=2,000,000g/mol; Stokes radius r_s= 26.1nm, calculated from $r_s=0.27 \cdot M_w^{0.498}$).

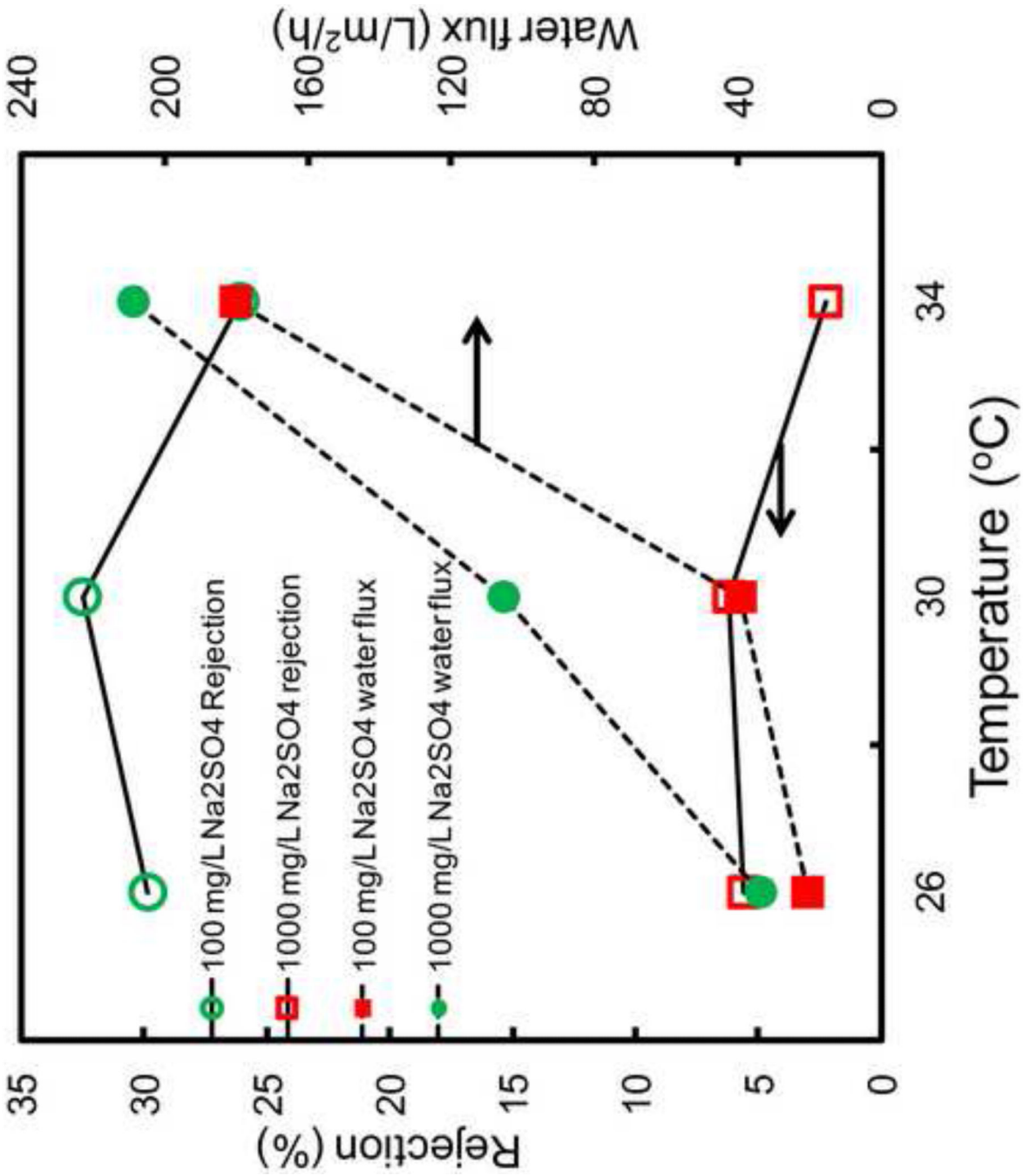

Figure 11.

Na_2SO4 rejection through PNIPAAm-FPAA-PVDFHE Sepro membrane at different temperatures (feed conc.=100 mg/L and 1000 mg/L, P=3.8 bar, pH=6.5).

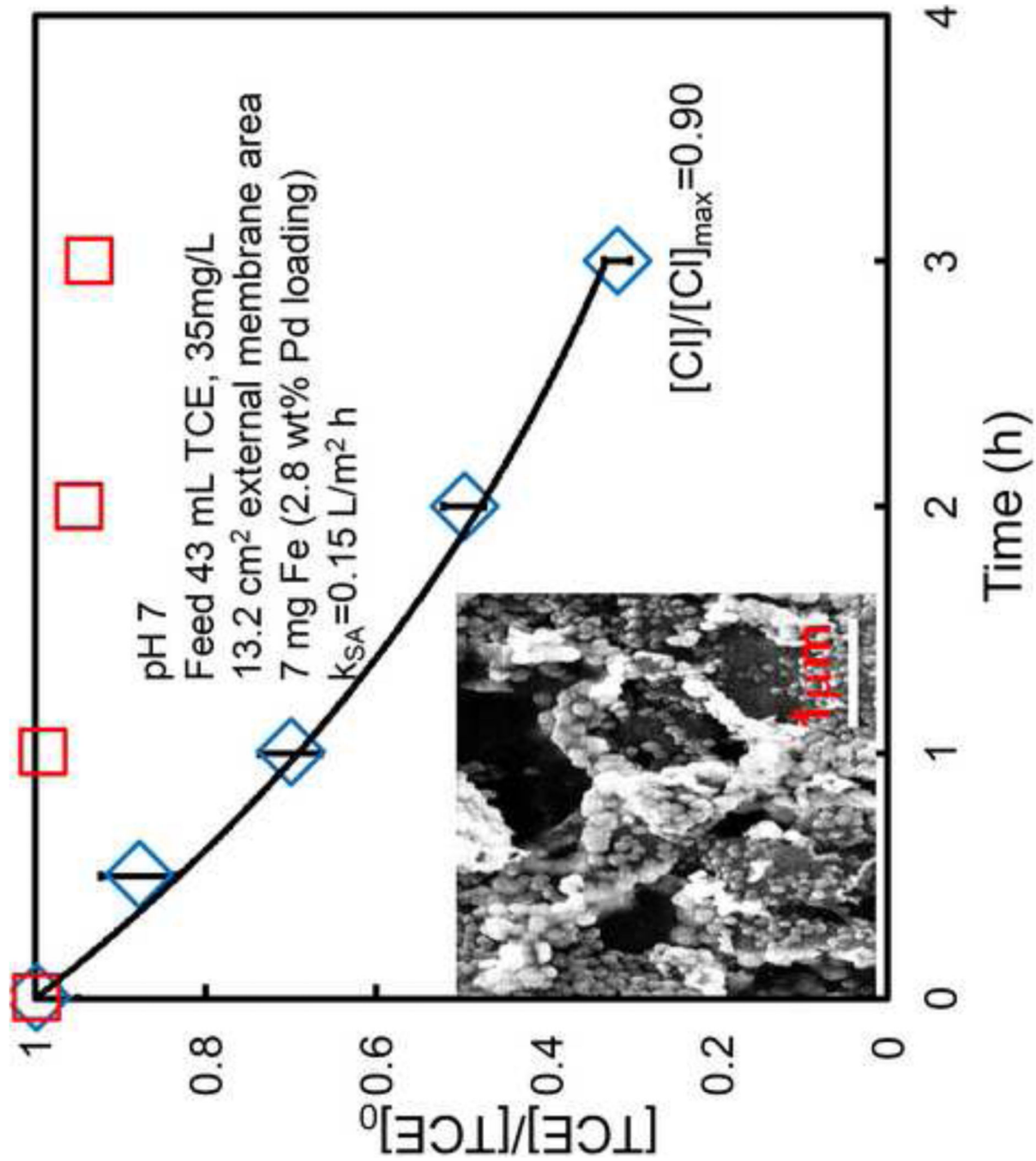

Figure 12.

TCE dechlorination using Fe/Pd nanoparticles (diamond symbols) in PNIPAAm-FPAA-PVDF Sepro membrane .The inset figure is the SEM image of nanoparticles in membrane pore. The diamond symbols represent the control experiment with only membrane (no metal particles).

Table 1

Functionalized Membranes Utilized in Experiments

Membrane abbreviation	Membrane full name
PNIPAAm-PVDF	PNIPAAm functionalized Millipore PVDF membrane in lab-scale
FPAA-PVDFHE	**Full-scale** PAA functionalized PVDFHE membrane by joint work with Sepro Inc. CA, USA
PNIPAAm-FPAA-PVDFHE	Post PNIPAAm functionalized FPAA-PVDFHE membrane in lab-scale